INTERNATIONAL JOURNAL OF PRECISION ENGINEERING AND MANUFACTURING-GREEN TECHNOLOGY Vol. 4, No. 2, pp. 211-219 APRIL 2017 / 211

REGULAR PAPER

DOI: 10.1007/s40684-017-0026-x
ISSN 2288-6206 (Print) / 2198-0810 (Online)

Nondestructive Evaluation of Hidden Damages in Glass Fiber Reinforced Plastic by Using the Terahertz Spectroscopy

Do-Hyoung Kim[1], Chung-Hyeon Ryu[1], Sung-Hyun Park[1], and Hak-Sung Kim[1,2,#]

1 Department of Mechanical Convergence Engineering, Hanyang University, 222, Wangsimni-ro, Seongdong-gu, Seoul, 04763, South Korea
2 Institute of Nano Science and Technology, Hanyang University, 222, Wangsimni-ro, Seongdong-gu, Seoul, 04763, South Korea
Corresponding Author / E-mail: kima@hanyang.ac.kr, TEL: +82-2-2220-4899, FAX: +82-2-2220-2299

KEYWORDS: Non-destructive evaluation, Glass fiber reinforced plastic, Delamination, Failure modes

In this work, the terahertz (THz) spectroscopy system was used for the detecting and evaluation of hidden damages in a glass fiber reinforced plastic (GFRP). The interaction between THz and the GFRP was analyzed including the effects of reflecting, scattering and absorption of THz radiations with respect to the type of hidden damage. Both the transmission and reflective configurations were used to investigate the hidden damages including the delamination, fiber fracture and moisture absorption. Finally, the hidden damages inside of the composite laminates were successfully imaged simultaneously based on the time-domain spectroscopy of THz radiation. Additionally, the moisture absorption damage in the GFRP could be detected by analyzing of the frequency domain spectrum. It is expected that the developed THz nondestructive evaluation (NDE) technique can be widely used to evaluate the health of the composite structures.

Manuscript received: August 23, 2016 / Revised: October 31, 2016 / Accepted: February 20, 2017

NOMENCLATURE

R_s = Reflectance for s-polarized THz wave
R_p = Reflectance for p-polarized THz wave
R = Reflectance for THz wave
T = Transmittance for THz wave
n_1 = Refractive index of incidence materials
n_2 = Refractive index of refraction materials
n = Refractive index
θ_1 = Incidence angle of THz wave
θ_2 = Refractive angle of the THz wave
A = Absorbance of refraction material
I_0 = Initial power of THz wave
x = Thickness of specimen
α = Absorption coefficient of refractive materials
ε_r = Relative permittivity of the material
μ_r = Relative permeability of the material

1. Introduction

The fiber reinforced composites are being widely used as structural components in various industries because they provide higher specific strength, stiffness, natural frequency and corrosion resistance to the structure compared to the other conventional metallic materials.[1-3] However, the reliability and mechanical properties of fiber composites can be weakened by various hidden defects and damages such as delamination, voids, fiber fracture or moisture absorption.[4] These can originate at any time by the inappropriate manufacturing processes as well as mechanical loads, impacts or harsh environmental using conditions. It is well known that they can lead to significant degradation of mechanical properties and a fatigue life of structure due to the poor structural integrity.[5] Therefore, appropriate inspection techniques are required to detect and characterize the hidden defects and damages in their inside in order to ensure the safe use of composite structures.[6,7]

There are a number of current nondestructive evaluation (NDE) techniques which have been widely deployed for the composite structures such as the X-ray, ultrasound wave, liquid penetrant and the others.[4] However, they suffer from some limitations for inspection of

the composite structures. For example, the use of x-rays is limited due to the safety considerations related with the high-energy radiation, and the requirements to have access to both sides of a composite part. In the case of ultrasound inspection, the coupling medium and requirements for reference standards have become the important limitations. Also, the liquid penetrant has the important problem because it can be used only for the detecting of defects on surface.[8] For these reasons, the terahertz (THz) wave has drawn much attention from researchers in related fields, which can overcome the limitations of conventional NDE techniques. The THz radiation (0.1 - 10 THz) can penetrate common nonmetallic materials, and offers noninvasive, noncontact, nonionizing method with a no health risk.[9] Also, it gives a broad range of information about the material properties.[10-12]

Because of the difficulty in generating and detecting of THz wave, only the little studies on interaction between the THz radiation and composite materials could be performed until a couple of years ago. In recent years, the basic researches of THz NDE for fiber reinforced composites have been allowed with the help of new advances in the THz generating and detecting technology based on the optical and electronic combining methods.[13] The THz spectroscopy has been investigated to detect the various defects in glass fiber reinforced plastic (GFRP) including the voids,[14] delamination,[14-17] bend damage,[6,18] and heat damage.[6,16,18] The detection of small voids in GFRP has been reported with the scattering effect of THz wave.[15] Also, the burn spot, bend damage and hidden voids of GFRP were could be detected by using the transmission and reflection configuration of THz with scattering approximations.[6,16,18] However, the NDE results have been limited to the relatively thin composite structure and the defects on near surface due to the low power of THz generation. Also, the hidden damages in composite have been imaged with the small scanning area or low scanning resolution because the fast and high scanning resolution of THz system could have not been available to be employed. In the case of delamination, the THz responses from the multiple delamination which made by using the polytetrafluoroethylene film were analyzed based on the basic optical theory of reflection and transmission.[17] Nevertheless, the analysis results of THz response from the GFRP specimen with various type of hidden damage developed from the mechanical load have not been reported.

In this study, the various hidden damages and defects including the fiber fracture, delamination, compressive damage and moisture absorption in the GFRP were simultaneously evaluated by using the pulsed THz spectroscopy imaging system. The interactions between THz and the GFRP were analyzed with respect to the type of hidden damages and thickness of specimen including the effects of reflecting, scattering and absorption of THz radiations. The whole area of GFRP specimen was inspected in a single scan by using both the transmission and reflective configurations to evaluate the various damages in GFRP. Based on the results of THz spectroscopy, the all of hidden damages in GFRP specimen were simulteneously imaged by high-resolution of two-dimensional images.

2. Experiments

2.1 Terahertz Inspection System

A THz radiation lies in the region of the electromagnetic spectrum between 100 GHz and 30 THz. This is the section overlapping the upper frequency range of the microwaves through the far infrared. For this reason, the THz offers a great advantage which is relatively low energy. Thus, it makes them biologically safe as well as non-damaging to materials, while it easily pass through many common non-metallic materials.[15] Additionally, the THz wave can be used not only for the imaging an object but also for the determination of its chemical makeup by interacting with molecular rotations and vibrations in condensed matter.[19] From in past years, the THz technology has received much attention as a NDE tool because of these unique properties.[19,20] In this study, the commercially available pulsed THz inspection system (FiCO, Zomega, USA) was used with the XY imaging module for the nondestructive evaluation of GFRP as shown in Fig. 1. In a pulsed type of THz system, the THz wave is emitted with the broad bandwidth, not the specific frequency. The THz inspection system has a spectral range from 100 GHz to 3 THz, with 11 GHz of frequency resolution and 20 fs of time resolution. All of systems were fully connected with fiber optics and the signal-to-noise ratio (SNR) is 60 dB, which has been reported by the acceptable power for fast real-time measurement.[21] The specification of laser generator for THz wave was listed in Table 1. The XY imaging process can be achieved by the set of motorized stages in X and Y directions. The maximum scaning area of XY imaging module is 150 mm × 150 with the 50 μm of resolution. Also, the THz system can be configured for the reflective mode or the transmission measurements. Fig. 2 shows a schematic diagram of a THz spectrometer, used for the reflective and the transmission mode. As shown in Fig. 2, the THz impulses from the emitter which were focused on the sample by a set of mirrors. Then the impulses are reflected or transmitted back through the boundaries of

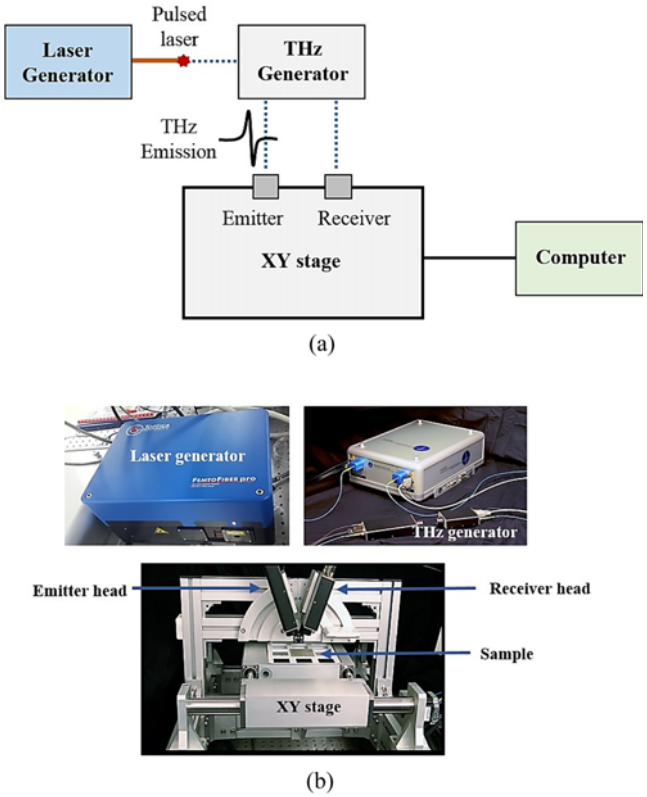

Fig. 1 THz inspection system: (a) Schematic diagram of the entire THz imaging system, (b) Detailed photograph of each components

Table 1 Specifications of laser generator in THz inspection system

Fundamental wavelength	1560 nm
Laser output power	> 350 mW
Pulse width	< 100 fs
Repetition rate	80 MHz
Beam divergence	< 2 mrad

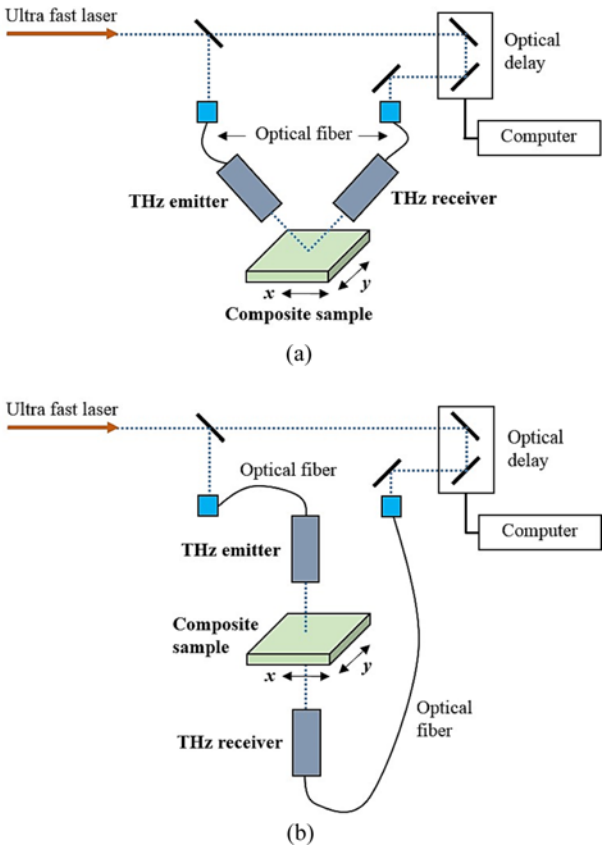

Fig. 2 A schematic diagram of THz spectroscopy system: (a) Reflective mode, (b) Transmission mode

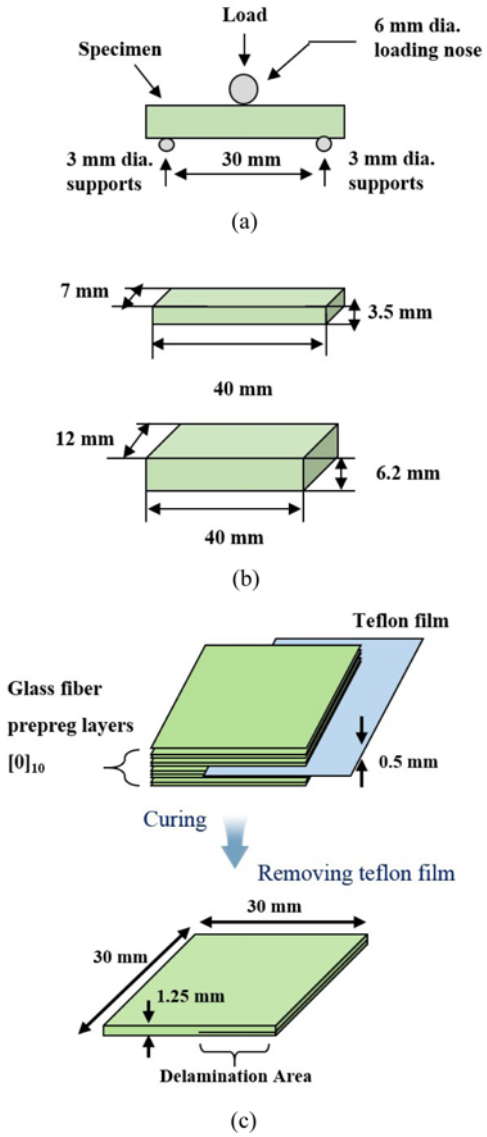

Fig. 3 A schematic diagram of GFRP specimen preparation: (a) Experiment condition of short-beam test, (b) Geometry of short-beam test specimens, (c) Manufacturing process of delaminated GFRP specimen

different refractive indices inside of sample. Then, the impulses gathered by a set of mirrors and fall onto the detector. The position and types of the hidden defects can be investigated based on the different wave response between reflected or transmitted signals of the THz waves for the determining of medium properties.[20] During the inspection, the repeatability could be achieved by installation of system which taking two consecutive data sets and normalizing their frequency spectra. This normalization gives about 99% data repeatability after 100 scans averaging for each data set in less than 1 second.

2.2. Sample Preparation

In this work, the GFRP specimens with various hidden damages were prepared by mechanical load. Firstly, the short-beam strength tests were performed based on ASTM standard (ASTM D2344) to make the mechanical damages in inside of the samples. The GFRP specimens were fabricated by using commercially available glass fiber prepreg (UGN 150, SK Chemical, South Korea) with 24 and 42 layers which have 3.5 mm and 6.2 mm of thickness, respectively. All of the composites were made by a hand layup method with unidirectional fiber direction. The schematic diagram of short-beam strength test and the specimens were represented as shown in Figs. 3(a) and 3(b). The short-beam test was performed by using the universal testing machine (KSU-5M, South Korea) with 1.0 mm/min of testing speed. After the experiment, the failure modes were observed by using a microscope.

Additionally, the hidden delamination in GFRP was made also from the manufacturing process. The delamination could be prepared by using the polytetrafluoroethylene film which had been inserted in the inside of GFRP layers before the curing process. Fig. 3(c) represents the manufacturing process of the delaminated GFRP specimen. After the curing process, the 0.5 mm thickness of delamination was made in the middle of specimen by removing the polytetrafluoroethylene film. Also, the moisture absorption was conducted for the delaminated specimen to evaluate the hygroscopic hidden damage by using the THz spectroscopy. In this work, the moisture was absorbed during 6 hours in a constant temperature bath to maintain a constant temperature at 80ºC.

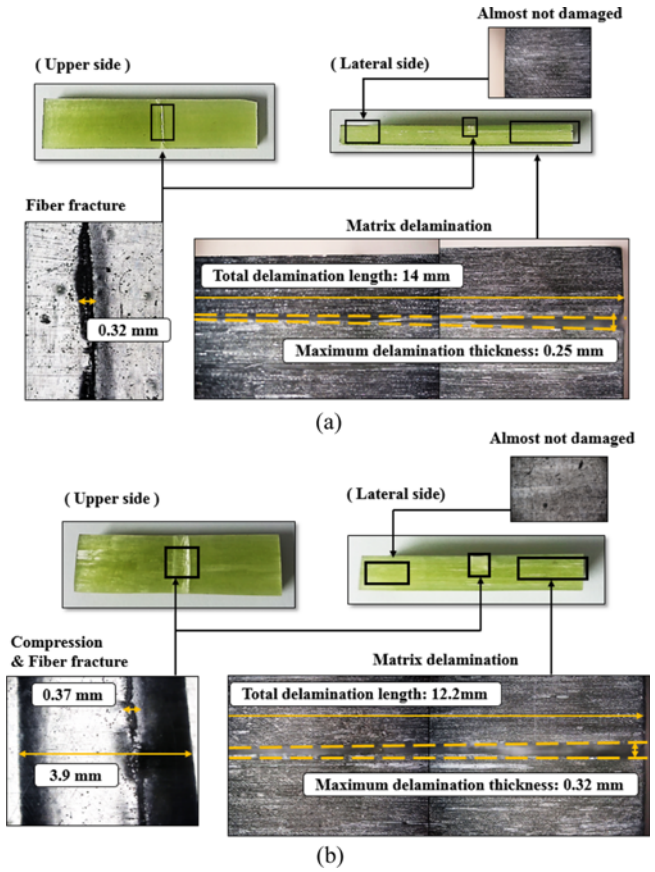

Fig. 4 Microscope images of short-beam tested GFRP specimens: (a) 3.5 mm thickness, (b) 6.2 mm thickness

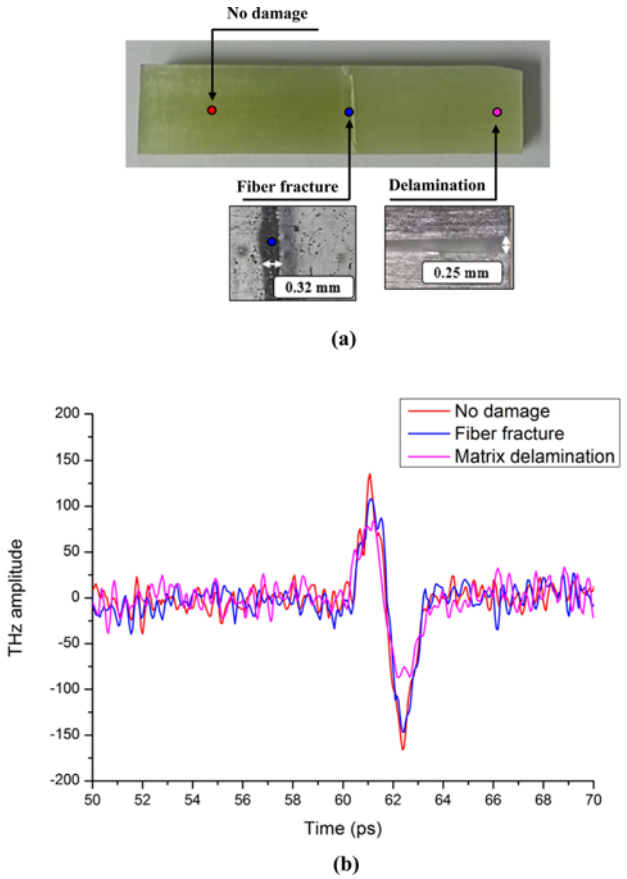

Fig. 5 THz inspection results of 3.5 mm thickness GFRP with respect to the failure position: (a) Position of inspection, (b) Change of THz amplitude

Finally, the scanning of THz radiation was performed for the each GFRP specimens. For the short-beam tested GFRP specimen, both the transmission and reflective configuration were used to investigate the various THz responds with respect to the type of hidden damage. The THz inspection was also performed for the GFRP specimen manufactured with the delamination by using the reflective configuration. For all of cases, the whole area of specimen was scanned by THz using the 50 μm of resolution. During the scanning, the wave information of each point was automatically saved in the computer. Especially, the measured THz signals from the moisture absorbed specimen were processed by Fast-Fourier Transform (FFT) to obtain frequency responses based on experimental report that the THz magnitude is much absorbed at specific frequency region by water molecules.[22] After the THz scanning, entire part of specimens was graphically imaged based on the peak-to-peak analysis of THz amplitude.

3. Results and Discussion

Fig. 4 shows the microscope images of GFRP specimens after the short-beam test. It was found that the delamination and the fiber fracture occurred in both cases of the 3.5 mm and the 6.2 mm thickness. In the case of 3.5 mm, the fibers of upper side were fractured and the matrix delamination was developed at single side of specimen. The gap of delamination was increased from the inside to outside direction. The similar failure modes were observed in the case of 6.2 mm but the compression failure additionally occurred due to the thick thickness of GFRP layer as shown Fig. 4(b). All of these hidden damages were evaluated by using the THz spectroscopy and compared to the microscope images.

Fig. 5(b) shows the THz inspection results of 3.5 mm thickness GFRP with respect to the failure position as shown in Fig. 5(a). It was found that the amplitude of THz wave was reduced at the damaged region. It is noteworthy that the THz amplitude was more decreased at the delamination area compared to that of the fiber fracture. The THz inspection was also performed from the inside to outside direction that the gap of delamination is increased as shown in Fig. 6(a). It could be known that he THz amplitude was much reduced from the delamination region, and also it was slightly decreased as the gap of delamination increases (Fig. 6(b)).

Fig. 7(a) shows the THz response from 6.2 mm thickness of GFRP with respect to the failure position as shown in Fig. 7(b). Similar to the results of 3.2 mm specimen, it was found that the THz amplitude was reduced in the damage regions. Additionally, the THz amplitude was decreased also at the region of compression damage. From these results, it can be concluded that the THz amplitude is reduced when it passes through the damaged region, and also that of reducing ratio is depending on its failure mode. It comes from the fact that the various optical effects of THz wave occurred when it passed through the damage region.[13] As shown in Fig. 8, if there are no defects in the material, two reflections (air/GFRP and GFRP/air) and one absorption

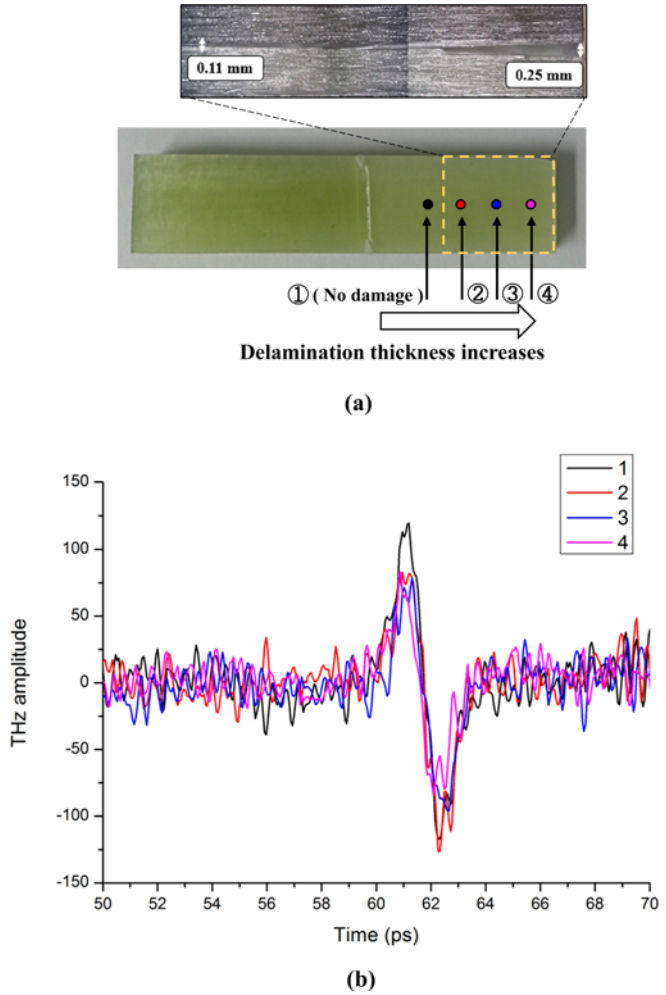

Fig. 6 THz inspection results of 3.5 mm thickness GFRP with respect to the delaminated thickness: (a) Position of inspection, (b) Change of THz amplitude

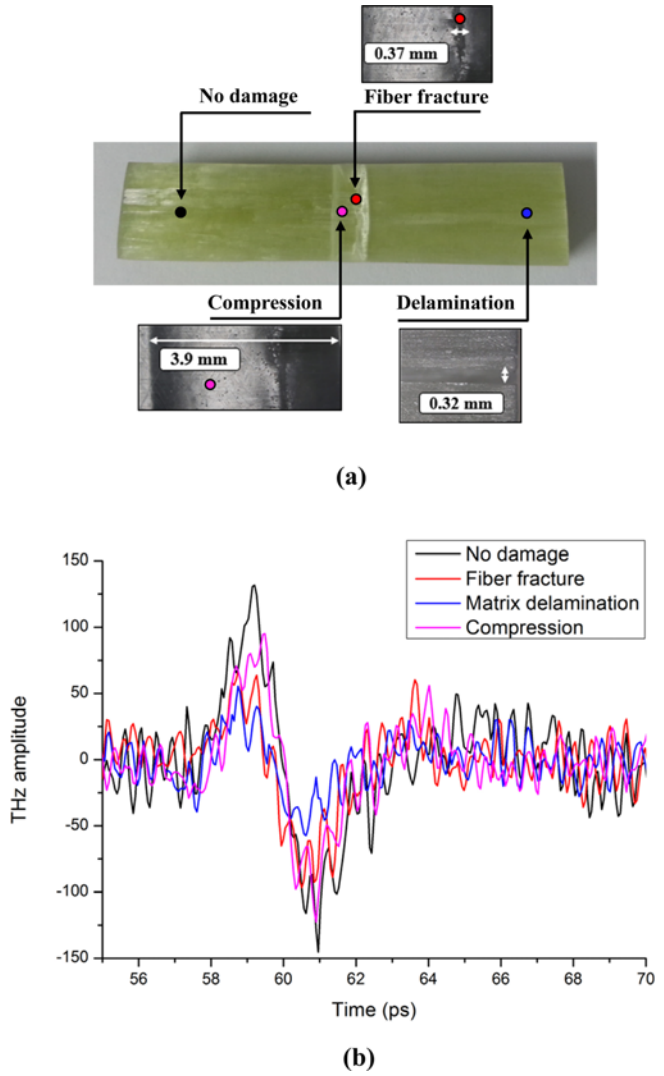

Fig. 7 THz inspection results of 6.2 mm thickness GFRP with respect to the failure position: (a) Position of inspection, (b) Change of THz amplitude

(in GFRP) occurred during the transmission. If there is small defect such as the fiber fracture, the THz wave loses more energy due to the scattering effect.[13] The scattering is well known from optics that the incident electromagnetic wave loses energy with producing of signals in random directions at the rough surface during the transmission.[23] In the case of large defect such as delamination, the THz loses more severe energy due to the additional interfaces between the fracture surfaces. This is the come from the fact that the additional reflection, scattering and energy absorption occurred from the interfaces. To investigate the change of amplitude in quantitative manner, the power of the THz waves was calculated by using the Fresnel equation as follows:[17]

$$R_s = \left| (n_1 \cos\theta_1 - n_2 \sqrt{1-(\sin\theta_1 \cdot n_1/n_2)})^2 \right. \\ \left. / (n_1 \cos\theta_1 + n_2 \sqrt{1-(\sin\theta_1 \cdot n_1/n_2)})^2 \right|^2 \quad (1)$$

$$R_p = \left| (n_1 \sqrt{1-(\sin\theta_1 \cdot n_1/n_2)} - n_2 cos\theta_1) \right. \\ \left. / (n_1 \sqrt{1-(\sin\theta_1 \cdot n_1/n_2)^2} + n_2 \cos\theta_1) \right|^2 \quad (2)$$

$$R = (R_s + R_p)/2 \quad (3)$$

$$T = 1 - R \quad (4)$$

where R_s is the reflectance for s-polarized THz wave, R_p is the reflectance for p-polarized THz wave, T is the transmittance for THz wave, n_1 is the refractive index of the incidence materials, n_2 is the refractive index of the refraction materials, θ_1 is the incidence angle of THz wave, and θ_2 is the refractive angle of THz wave. It has been reported that the refractive index of the GFRP is known to be 2.1, while that of air is 1 in the THz region.[24-26] Also, the absorbed power of THz wave can be calculated by following equation:

$$A = I_0(1 - e^{-\alpha x}) \quad (5)$$

where A is the absorbance of refraction material, I_0 is the initial power of THz wave, x is the thickness of specimen and α is the absorption coefficient of the refractive materials. In the delamination region, the additional two reflections and one absorption of THz wave occurred

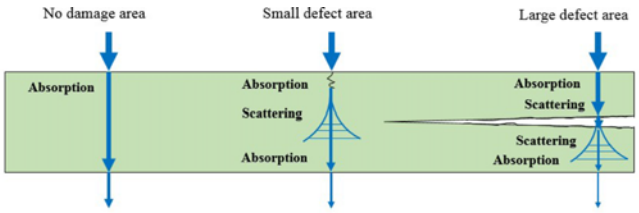

Fig. 8 Optical effects of THz wave in GFRP specimen when using transmission mode with respect to the type of hidden damage

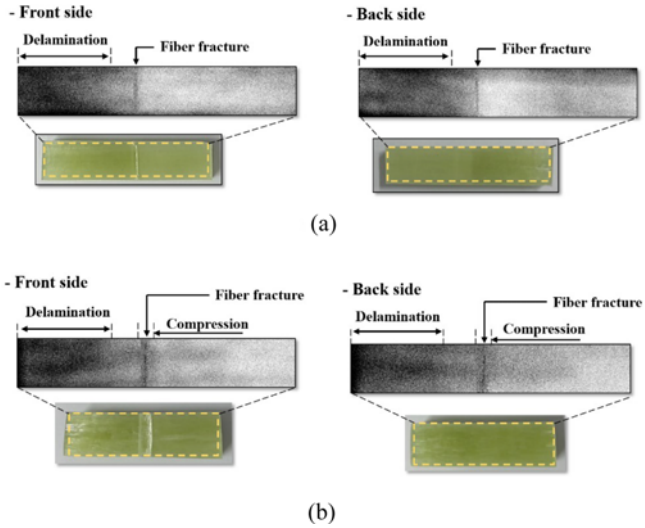

Fig. 9 Damage detecting of GFRP specimen based on the results of THz spectroscopy using transmission mode: (a) 3.5 mm thickness, (b) 6.2 mm thickness

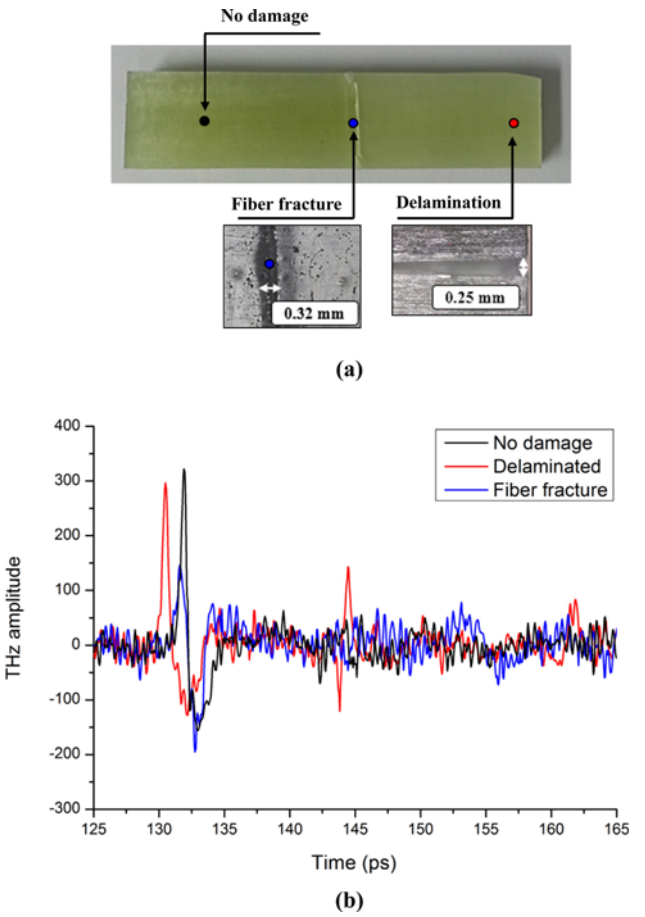

Fig. 10 THz inspection results of 3.5 mm thickness GFRP using reflective mode with respect to the failure position: (a) Position of inspection, (b) Change of THz amplitude

from separated bottom part of GFRP due to the delamination (Fig. 8). By using above equations, the reduced THz amplitude in the delamination region was calculated to be about 78% of the amplitude in the no damage region. However, the amplitude should be more decreased because the surfaces between delamination are not a flat clean surfaces which lead to the scattering of THz wave. Additionally, the amplitude was more reduced as the gap of delamination increases due to the extended distance of diffusion or re-scattered radiations between two scattering surfaces.[23] These are the reason that the THz amplitude was more decreased as the gap of delamination is increased (Figs. 5(b), 6(b) and 7(b)). In the case of compression damage, the amplitude was slightly reduced compared to the no damage region. It may come from the fact that the scattering of THz wave occurred due to the micro cracks in inside of GFRP which generated under the compression load (Fig. 7(b)).

Fig. 9 shows the THz scanning images for short-beam tested GFRP specimens. As shown in the pictures, the delamination and fiber fracture inside of specimen were successfully imaged based on THz spectroscopy in the both thickness cases. It is noteworthy that both the delamination and fiber fracture could be successfully detected from the bottom side of specimen, as well as the upper side. The gap of the delamination could be successfully differentiated by the contrast in scanning results. Additionally, the compression damage also could be detected from the both side in the cased of 6.2 mm thickness. Based on these results, it can be concluded that the various hidden damages in GFRP specimen could be successfully evaluated by using the THz inspection system with transmission configuration.

Fig. 10(b) shows the THz response from 3.5 mm thickness of short-beam tested specimen in reflective configuration with respect to the failure position (Fig. 10(a)). It was found that the different THz responses were obtained as the types of hidden damage. First of all, the front peak was obtained which reflected from the surface of specimen (130 - 135 ps). It could be known that the all of front peaks showed reversed phase compared to the transmitted THz wave (Fig. 5(b)), because the fixed reflection occurred from the low density medium (air) to the high density medium (GFRP). For this case, the relative permittivity can be obtained by using the following equation from the refractive index of the GFRP:

$$\varepsilon_r = n^2/\mu_r \tag{6}$$

where ε_r is the relative permittivity of the material, μ_r is the relative permeability of the material, and n is the refractive index. In the case of the paramagnetic and diamagnetic materials, the relative permeability is approximately 1.[27] Therefore, the relative permittivity could be determined to be 4.41, while that of air is 1. Additionally, the front peak was moved forward at the delamination region because the

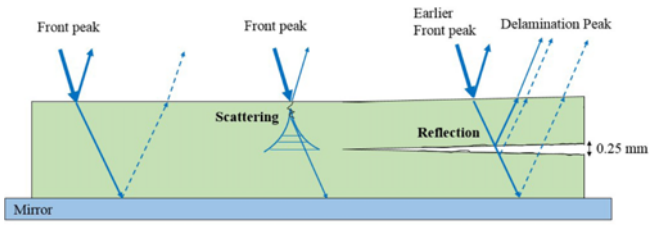

Fig. 11 Optical effects of THz wave in GFRP specimen when using reflective mode with respect to the type of hidden damage

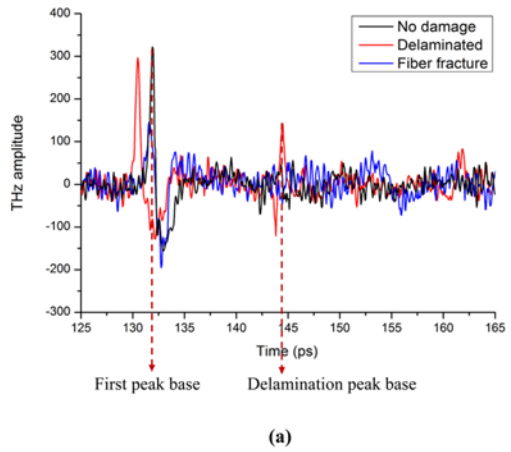

Fig. 12 Damage detecting of 3.5 mm thickness GFRP specimen based on the results of THz spectroscopy using reflective mode: (a) Imaging basis, (b) Images

travel distance of THz wave from the emitter to detector was slightly reduced due to the lifted surface of specimen as shown in microscopic image of delamination (Fig. 10(a)). Also, it is noteworthy that another reflected peak was detected at 145 ps from the delamination region. It was come from the fact that the additional reflection occurred due to the fractured interfaces of matrix delamination. The schematic of detailed THz spectroscopy in the reflective mode was depicted in Fig. 11. The earlier front reflection occurred due to the lifted surface and the additional reflection occurred from the surface of delamination (GFRP/air). Also, the reversed phase of delamination peak compared to the front peak showed the fact that the THz wave was reflected from the upper interface of delamination, because the free reflection occurred when the THz wave passes from the high density medium (GFRP) to the low density medium (air). In the case of fiber fracture, the amplitude of front peak was much reduced (Fig 10(b)). As shown in Fig. 11, it is because the THz wave lost much energy during reflection due to the scattering effect at the rough surface of fracture, compared to that of no damage region. Based on these results, the hidden

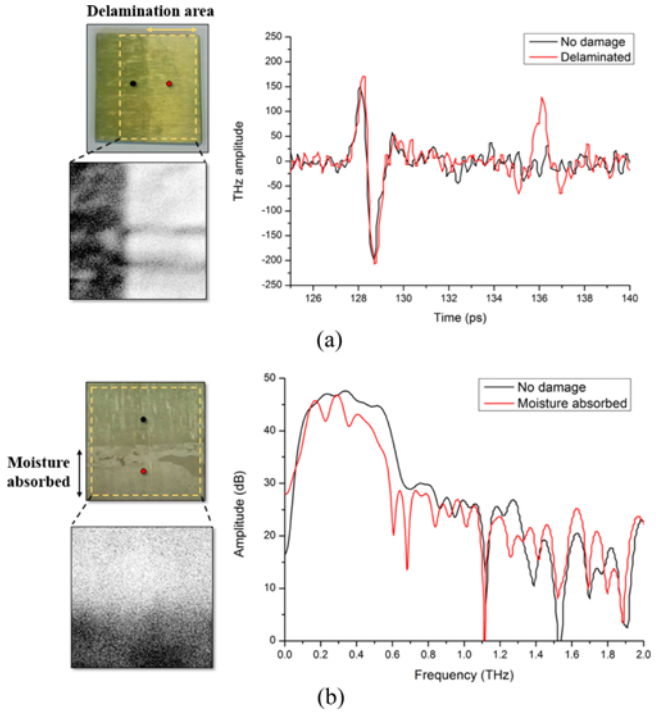

Fig. 13 Damage detecting of delaminated GFRP specimen based on the results of THz spectroscopy using reflective mode: (a) Delamination, (b) Moisture absorption

damages in specimen could be imaged as shown in Fig. 12. Based on these results, the THz imaging was performed based on the both of different respond of first peak (132 ps) and delamination peak (144 ps), respectively. It was found that the fiber fracture and matrix delamination could be detected successfully by using the THz inspection system with reflective mode.

Fig. 13 shows the results of THz spectroscopy and image scanning of GFRP specimen with delamination which developed from the manufacturing process by using the polytetrafluoroethylene film. As shown in Fig. 13(a), the reversed front peaks were detected which were reflected from the surface of specimen. Also, similar to the short beam tested specimen, the additional THz respond was observed from 54 to 57 ps due to the delaminated surfaces. In this case, the different phase of delamination peak could be observed which was merged both of reflected from upper GFRP/air interface (free reflection) and bottom air/GFRP interface (fixed reflection). This is because the second delamination peak could be detected due to the thin thickness of specimen compared to the short-beam tested specimen. Based on these results, the delamination area could be successfully imaged.

Fig. 13(b) shows the results of THz spectroscopy and scanned images of moisture absorbed GFRP specimen. As shown in Fig. 13(b), it was found that the amplitude of THz was broadly reduced in the frequency range from 100 GHz to 1.1 THz at the moisture absorbed region. This is because the power of THz wave could be easily absorbed by the water molecules. Especially, the THz amplitude was much absorbed at 0.55 and 0.75 THz frequency region by water molecules, similar to the results of Xin at al.[22] Meanwhile, it can be seen that the amplitude of THz waves were much attenuated from about 1.1 THz region. This is because the power of THz wave was

much weakened from about 1.1 THz due to the limit of laser generator used in this study. However, the significant analysis of THz wave in frequency domain could be conducted by using the frequency range from 100 GHz to 1.1 THz. As shown in Fig. 13(b), the moisture absorbed region in specimen was successfully imaged based on the different amplitude at 0.7 THz of frequency area. Based on these results, it can be concluded that both the matrix delamination and moisture absorption of GFRP also could be successfully evaluated by using devised THz inspection system.

4. Conclusions

In this work, the THz spectroscopy imaging system was used for detecting and evaluating of hidden damages in the GFRP. The interaction between THz and the GFRP was discussed with respect to the type of hidden damages including the effects of reflecting, scattering and absorption of THz radiations. Also, the hidden damages such as matrix delamination, fiber breakage, compression and moisture absorption inside of the GFRP were successfully detected based on results of THz spectroscopy. It is expected that the THz nondestructive evaluation (NDE) technique can be widely used to evaluate the health of the composite structures.

ACKNOWLEDGEMENT

This work was supported by the National Research Foundation of South Korea (NRF) funded by the Ministry of Education (No. 2012R1A6A1029029 and 2013M2A2A9043280).

REFERENCES

1. Beardmore, P., “Composite Structures for Automobiles,” Compos Struct, Vol. 5, No. 3, pp. 163-176, 1986.
2. Asnafi, N., Langstedt, G., Andersson, C.-H., Östergren, N., and Håkansson, T., “A New Lightweight Metal-Composite-Metal Panel for Applications in the Automotive and Other Industries,” Thin-Walled Structures, Vol. 36, No. 4, pp. 289-310, 2000.
3. Beardmore, P. and Johnson, C., “The Potential for Composites in Structural Automotive Applications,” Composites Science and Technology, Vol. 26, No. 4, pp. 251-281, 1986.
4. Kapadia, A., “Non Destructive Testing of Composite Materials,” National Composites Network, pp. 1-4, 2007.
5. Mangalgiri, P., “Composite Materials for Aerospace Applications,” Bulletin of Materials Science, Vol. 22, No. 3, pp. 657-664, 1999.
6. Stoik, C., Bohn, M., and Blackshire, J., “Nondestructive Evaluation of Aircraft Composites Using Reflective Terahertz Time Domain Spectroscopy,” NDT&E International, Vol. 43, No. 2, pp. 106-115, 2010.
7. Shull, P. J., “Nondestructive Evaluation: Theory, Techniques, and Applications,” CRC Press, 2016.
8. Summerscales, J., “Non-Destructive Testing of Fibre-Reinforced Plastics Composites,” Springer Science & Business Media, 1990.
9. Lee, Y.-S., “Principles of Terahertz Science and Technology,” Springer Science & Business Media, 2009.
10. Chan, W. L., Deibel, J., and Mittleman, D. M., “Imaging with Terahertz Radiation,” Reports on Progress in Physics, Vol. 70, No. 8, pp. 1325, 2007.
11. Wang, S. and Zhang, X. C., “Pulsed Terahertz Tomography,” Journal of Physics D: Applied Physics, Vol. 37, No. 4, pp. R1-R36, 2004.
12. Wietzke, S., Jordens, C., Krumbholz, N., Baudrit, B., Bastian, M., et al., “Terahertz Imaging: A New Non-Destructive Technique for the Quality Control of Plastic Weld Joints,” Journal of the European Optical Society-Rapid Publications, 2007.
13. Anbarasu, A., “Characterization of Defects in Fiber Composites Using Terahertz Imaging,” M.Sc. Thesis, Georgia Institute of Technology, pp. 1-42, 2008.
14. Png, G. M., “Terahertz Spectroscopy and Modelling of Biotissue,” Ph.D. Thesis, University of Adelaide, 2010.
15. Im, K.-H., Hsu, D. K., Chiou, C.-P., Barnard, D. J., Jung, J.-A., et al., “Terahertz Wave Approach and Application on FRP Composites,” Advances in Materials Science and Engineering, Article ID: 563962, 2013.
16. Stoik, C. D., Bohn, M. J., and Blackshire, J. L., “Nondestructive Evaluation of Aircraft Composites Using Transmissive Terahertz Time Domain Spectroscopy,” Optics Express, Vol. 16, No. 21, pp. 17039-17051, 2008.
17. Ryu, C.-H., Park, S.-H., Kim, D.-H., Jhang, K.-Y., and Kim, H.-S., “Nondestructive Evaluation of Hidden Multi-Delamination in a Glass-Fiber-Reinforced Plastic Composite Using Terahertz Spectroscopy,” Composite Structures, Vol. 156, pp. 338-347, 2016.
18. Stoik, C. D., “Nondestructive Evaluation of Aircraft Composites Using Terahertz Time Domain Spectroscopy,” Optics Express, Vol. 16, No. 21, pp. 17039-17051, 2008.
19. Ferguson, B. and Zhang, X. C., “Materials for Terahertz Science and Technology,” Nature Materials, Vol. 1, No. 1, pp. 26-33, 2002.
20. Mittleman, D. M., Gupta, M., Neelamani, R., Baraniuk, R. G., Rudd, J. V., et al., “Recent Advances in Terahertz Imaging,” Applied Physics B, Vol. 68, No. 6, pp. 1085-1094, 1999.
21. Saeedkia, D., “Handbook of Terahertz Technology for Imaging,” Sensing and Communications, Elsevier, 2013.
22. Xin, X., Altan, H., Saint, A., Matten, D., and Alfano, R. R., “Terahertz Absorption Spectrum of Para and Ortho Water Vapors at Different Humidities at Room Temperature,” Jouranl of Applied Physics, Vol. 100, No. 9, Paper No. 094905, 2006.
23. Swift, G. P., Dai, D., and Fletcher, J. R., “Terahertz Scattering: Comparison of a Novel Theoretical Approach with Experiment,” Proc. of International Society for Optics and Photonics in Integrated Optoelectronic Devices, 2006.

24. Im, K.-H., Lee, K.-S., Yang, I.-Y., Yang, Y.-J., Seo, Y.-H., et al., "Advanced T-Ray Nondestructive Evaluation of Defects in FRP Solid Composites," Int. J. Precis. Eng. Manuf., Vol. 14, No. 6, pp. 1093-1098, 2013.

25. Rutz, F., Koch, M., Khare, S., Moneke, M., Richter, H., et al., "Terahertz Quality Control of Polymeric Products," International Journal of Infrared and Millimeter Waves, Vol. 27, No. 4, pp. 547-556, 2006.

26. Park, J.-W., Im, K.-H., Yang, I.-Y., Kim, S.-K., Kang, S.-J., et al. "Terahertz Radiation NDE of Composite Materials for Wind Turbine Applications," Int. J. Precis. Eng. Manuf., Vol. 15, No. 6, pp. 1247-1254, 2014.

27. Yang, T., Brown, R., Kempel, L., and Kofinas, P., "Controlled Synthesis of Core-Shell Iron-Silica Nanoparticles and their Magneto-Dielectric Properties in Polymer Composites," Nanotechnology, Vol. 22, No. 10, Paper No. 105601, 2011.